PNAS
www.pnas.org

Supplementary Information for

Solar Thermal Desalination as a Nonlinear Optical Process

Pratiksha D. Dongare[#], Alessandro Alabastri[#], Oara Neumann, Peter Nordlander, and Naomi J. Halas

[#]Equal contribution

Peter Nordlander
Email: nordland@rice.edu
Naomi J. Halas
Email: halas@rice.edu

This PDF file includes:

Supplementary text
Figs. S1 to S20
References for SI reference citations

www.pnas.org/cgi/doi/10.1073/pnas.1905311116

Supplementary Information Text

1. Saturation vapor pressure of water – temperature dependence

The saturation vapor pressure of water can be fitted using the Antoine equation as:

$$p_{sat}(T) = 10^{A-B/(T+C)}$$

Where T is expressed in °C. In the following plot, tabulated water vapor pressures between 20 °C and 90 °C are compared with the fitting employing Antoine equation and with an exponential fit considered as:

$$p_{sat}(T) = p_0 e^{\gamma T}$$

Where T is expressed in °C. See Fig. S1.

2. Exponential dependence of water vapor concentration on intensity:

A rigorous expression for the temperature dependence of saturation vapor pressure of water, p_{sat}, can be obtained from the second law of thermodynamics by integrating the Clausius-Clapeyron equation(1) and can be well-approximated by an exponential relation. The water vapor concentration, c, at any point of the membrane surface is given by $c = \frac{P_{sat}(T)}{RT}$, where R is the ideal gas constant, and T is the temperature. To calculate the vapor flux, we calculate the concentration gradient ∇c across the membrane at each point and apply Fick's first law, which reads: $F = -MD\nabla c$, where F is the flux, M is the water vapor molar mass and D is the diffusion co-efficient of vapor in the membrane. Here, for simplicity, we consider average values of c for the membrane-water channel interface at the top (c_{top}) and bottom (c_{bottom}) of the membrane. We assume a linearly decreasing concentration across the membrane thickness with slope k given by $k = -\frac{c_{top}-c_{bottom}}{t_{memb}}$, where t_{memb} is the thickness of the membrane. In all our experiments we have faster distillate speed, 50 mL/min, compared to feed speed,5 mL/min. If the distillate flows much faster than the feed, as is the case here, it efficiently removes heat from the membrane-distillate interface, allowing us to assume a constant temperature $T \sim T_{amb}$ at the bottom surface. This allows us to write,

$$F(T) = c_{top}(T)\frac{MD}{t_{memb}} - c_{bottom}\frac{MD}{t_{memb}} \quad (1)$$

Neglecting constants, we have$F(T) \propto c_{top}(T) = c(T)$. We also want to keep the temperatures in the system in the range of 20-90 °C, i.e. 293.15-363.15 K, to avoid wetting the membrane near the boiling point of water. In this temperature range the RT term in $c = \frac{P_{sat}(T)}{RT}$ varies much less than $P_{sat}(T)$, i.e. $\frac{P_{sat}(363.15\ K)}{P_{sat}(293.15\ K)} > 20 \cdot \frac{R\cdot(363.15\ K)}{R\cdot(293.15K)}$. We can then consider RT a constant in the following discussion, so that $c = \frac{P_{sat}(T)}{RT} \propto f(T)$ where f(T), a function of temperature, contains the saturation pressure dependence on temperature. Assuming now that the temperature T of the membrane top surface increases linearly with illumination intensity I, flux rate F becomes proportional to f(I), a function of intensity. These assumptions are employed here only to present the general concept and are relaxed in the numerical model which considers all the relevant physical mechanisms (see ref(2) and methods section).

The next step of the analysis is to consider the effect of a lens array on this flux rate. Here, we consider a lens of focusing power M, calculated from the ratio of the lens area (A_{lens}) to the focal spot area (A_{focus}), given as: $M = \frac{A_{lens}}{A_{focus}} = \frac{{d_{lens}}^2}{{d_{focus}}^2}$, where d_{lens} and d_{focus} are the diameters of the lens and focal spot respectively. Considering the conventional exponential dependence of water vapor saturation pressure, $p_{sat}(T)$, on temperature and thus intensity, we get, $f(I) \propto e^{\alpha I}$,where α

is a constant. In the case of a lens array addition, one would then have the exponentially dependent flux rate (F_{exp}) as: $F_{exp} \propto \frac{e^{\alpha M I_0}}{M}$, where the effective intensity I has been substituted by background intensity I_0 (e.g. natural sunlight) multiplied by the lens focusing power M. Appearance of M in the denominator in the expression for F_{exp}, arises from the assumption that the area outside the focal spot is not illuminated by sunlight and has to be excluded from the average flux rate calculation. However, when considering an artificial linear dependence of water vapor saturation pressure, $p_{sat}(T)$, on temperature, and thus intensity, we have: $f(I) \propto \beta I$, where, β is constant. The linearly dependent flux (F_{lin}) in this case becomes $F_{lin} \propto \frac{\beta M I_0}{M} = \beta I_0$. While F_{exp} increases with M, F_{lin} is independent of the focusing power of the lens as M simplifies. While the physical framework described above is approximate, it conveys the general idea of the photon redistribution mechanism at the base of NESMD flux rate increase when lenses are employed.

While the relationship between temperature and intensity can be complicated with many variations across different systems, the concept applies, in principle, to any photothermal system where the sought average output per unit area (O) has a $O \propto T^n$ dependence with $T^m \propto I$ and $n > m$. In fact, by considering a power collecting area, A_{coll}, and an active area, $A_{act} = A_{coll}/M$, then A_{act} receives an intensity $I = MI_0$, where I_0 is the incident intensity. The condition $n > m$ guarantees that when $m > 0$ (i.e. when a T dependence exists), the average output $O \propto \left(\frac{A_{act}}{A_{coll}}\right) T^n = M^{\frac{n-m}{m}} I_0^{n/m}$ increases with magnification and thus benefits from the intensity redistribution of a fixed input power $P = A_{coll} I_0$.

3. Effect of CB coating thickness and absorption on membrane flux:

The darkness of the CB coating on the PVDF membrane is monitored by visual observation and thus the actual CB coating penetration depth on top of the PVDF membrane surface can vary. The PVDF membrane surface is also non-uniform and porous, serving as an additional variability factor for the resulting CB coating thickness. Theoretical analysis of the effect of absorption coefficient and CB coating thickness on the purified water flux as shown in Fig. S4 serves as a guideline to the experimentally obtained purified water flux values. We use an average of flux values for a coating thickness range of 2-5 microns and absorption coefficient of 3200 cm^{-1} (obtained from Fig. S4) for experimental flux comparison.

4. Efficiency of solar thermal distillation:

The efficiency of a solar thermal distillation system of area A, under sunlight intensity I_0 can be expressed as:

$$\eta = \frac{\dot{m}\, h_{ev}}{I_0 A},$$

Where $\dot{\mathbf{m}}$ is the measured mass loss rate for the evaporated water and $\mathbf{h_{ev}}$ is the evaporation enthalpy of water $\dot{\mathbf{m}} = \widetilde{\mathbf{F(I)}} \cdot \mathbf{A}$, where $\widetilde{\mathbf{F(I)}}$ is the intensity dependent average distilled water flux value that is reported in the manuscript in the units $kg/m^2 \cdot h$. It is calculated by integrating the flux at each point on the light absorbing membrane over the whole membrane area.

5. Effect of magnification factor on flux and maximum temperature in the system:

Reducing the focus diameter of the lens array increases the magnification factor (M) in the system because $M = \frac{D^2}{d^2}$ where, D is the diameter of the focusing lens and d is the dimeter of the focal spot. Therefore, reducing the focal spot diameter (d) results in increase of the flux in the

system as shown in Fig. S8a for 4" × 8" NESMD and Fig. S8b for 4" × 16" NESMD. This increase happens for both lens arrays with 1" and 2" lens diameters (D). The increase in flux is higher for the 2" lens array compared to the 1" lens array as the magnification factor is higher for the same focal spot dimeter. The increase in flux happens because of the nonlinear dependence of the saturation pressure of water vapor on temperature. The corresponding temperatures for 4" × 8" NESMD and 4" × 16" NESMD with 1" and 2" lens arrays are shown in Fig. S8c and S8d respectively.

6. Variation of flux and temperature with magnification for linear and exponential temperature dependence of saturation pressure:

For linear dependence of saturation pressure on temperature the purified water flux through the membrane does not change with the magnification factor (M) as shown in Fig. S10. The curve just moves up or down on the flux axis depending on the slope of the linear relation (Fig. S10). Figure S10 shows flux vs M curves for slopes of 130 (dashed black line with hollow squares) and 260 (dashed black line with hollow triangles). The flux vs M relation for exponential dependence is shown with the solid black line with solid squares in Fig. S10a. The temperatures in the linear dependence case for slope of 130 (dashed red line with hollow squares) and slope of 260 (dashed red line with hollow triangles) are very similar and in fact higher than the temperatures in the exponential dependence case (solid red line with solid squares). The feed input temperature is 293.15 K (20 °C) in all cases. The analysis of the feed output temperature with M for the linear case with slope of 130 (dashed red line with hollow squares), slope of 260 (dashed red line with hollow triangles), and exponential case (solid red line with solid squares) is shown in Fig. S10b. The feed output temperature reduces with M for the exponential case whereas it is almost constant above the magnification of 40 in linear case showing reduction in losses from the system with increasing magnification in the exponential dependence. It should be noted that some temperature ranges (and thus magnifications) exhibit larger fluxes if linear slopes are large enough. For example, the linear 'slope 260' case gives higher saturation pressures (Fig. S10c) below a threshold temperature of ~320 K, translating in larger fluxes for smaller magnifications (Fig. S10a). Flux rate variations with magnification is an indication of non-linearity at play in our system.

7. Nonlinear temperature increase with magnification

The hypothesis of linear temperature increase with increasing magnification holds in a simplified system described by a thin disk which homogeneously absorbs heat (Q_{abs} $[W/m^3]$) in its volume (V) and dissipates heat through its surfaces (total area A) by conduction and/or convection (let's call h $[W/(m^2K)]$ the generalized heat transfer coefficient). In steady state the total power absorbed by the disk has to be equal to the dissipated power. Let's consider a heated disk with radius r and height H, then $P_{abs} = Q_{abs}V = P_{out} = hA(T - T_{amb})$. By taking account the magnification ($M = R^2/r^2$) from a hypothetic lens of radius R, then $Q_{abs} = Q_0 M = Q_0 R^2/r^2$, where Q_0 is the natural absorption rate (the case where non lenses are employed in our case). Substituting now $V = \pi r^2 H$ and $A = 2\pi(r^2 + rH)$ we have $Q_0 R^2 H = 2(r^2 + rH)h(T - T_{amb})$. Being $r^2 = R^2/M$, if $r \gg h$ then $T - T_{amb} = \Delta T \cong MQ_0 H/2h \propto M$, that shows how the temperature increases linearly with magnification. While the focusing region in our system can be considered as a heated thin disk ($t_{disk} \approx 5$ μm), the dissipation process is less ideal as the disk is in contact with the rest of the membrane and, importantly, with the feed channel which, being thicker than the disk ($t_{channel} \approx 2$ mm) contributes with the heat dissipation, leading to smaller values of ΔT for increasing magnification. Fig. S11 shows the maximum temperature reached in a system composed of heated thin water disk (symbolizing the $t_{disk} = 5$ μm hot spot region) where a second cylinder (symbolizing the feed water channel with varying thickness $t_{channel}$ between 500 nm and 2.5 mm) has been placed in contact with its top surface. The thin disk (with

radius $r = R/\sqrt{M}$) is heated by a homogeneous $Q_{abs} = Q_0 M$ with $Q_0 = 1\,MW/m^3$. All the surfaces contribute to heat dissipation through an outward heat flux $q = h(T - T_{amb})$, $h = 5\,W/(m^2K)$. If the thickness of the channel is much smaller than the disk (blue line), then the channel has almost no effect and the linear trend obtained before is found. However, when channel thickness is increased the maximum temperature exhibits a sub-linear trend with respect to the magnification, M.

8. Reynolds number for the investigated system

Our model assumes a laminar flow for the feed and distillate channels. This choice is justified by low Reynolds numbers calculated for the system. For rectangular ducts, the transition to turbulent regime has been estimated at more than ~2500(3). Reynolds number is defined as(4):

$$Re = \frac{Lv\rho}{\mu}$$

Where L is the characteristic length of the system and v, ρ, μ are the characteristic velocity, density and dynamic viscosity of the fluid respectively. For a rectangular duct, the characteristic length can be substituted by the hydraulic diameter $D_H = 4A/P$ where A and P are the cross sectional area and perimeter wetted by the fluid. In our case channels have thickness $t_c = 2mm$ and width $w_c = 4in$ leading to a $L = D_H = 2(w_c t_c)/(w_c + t_c) \approx 5mm$. The maximum characteristic velocity has been considered as the nominal velocity in the higher velocity distillate channel $v = v_d \approx 3mm/s$. Temperature dependences of the density and dynamic viscosity of water have been considered in $\rho = \rho_w(T)$(1) and $\mu = \mu_w(T)$. In Fig. S13 the values for the Reynolds number between 293 K and 363 K are shown.

9. Flux dependence on magnification – net effect of saturation pressure

Many parameters describing our system depend on temperature (see Fig. S15 and Fig. S16). However, when all of them are considered constant at room temperature with the exception of the water vapor saturation pressure dependence, flux and maximum temperature trends follow a very similar trend to the ones reported in the main text. This confirms the main role played by the water vapor pressure in determining the performance of thermal desalination under different focusing conditions. See Fig. S17.

10. Solar intensity needed with and without lens array focusing to maintain the flux:

Considering a 4" × 8" NESMD system, Fig. S18 shows the intensity needed with 2" diameter lens array incorporation with NESMD (left axis) for varying focal spot diameters of 15 mm (light grey triangles), 10 mm (grey triangles), and 5 mm (dark grey triangles). The x-axis shows the intensity needed without the multilens array to obtain the same flux. The same flux can be obtained with lower intensities using lens array with NESMD as shown on y-axis. With 5 mm focal spot diameter with a 2" diameter lens array, the flux obtained at solar intensity of ~ 600 W/m^2 is similar to flux obtained at ~ 900 W/m^2 without lens array incorporation.

11. Maximum temperature variation with intensity for varying ambient temperatures:

Maximum temperature in a 4" × 16" NESMD system with (solid lines) and without (dashed lines) 2" lens array focusing with 5 mm focal spot diameter is shown in Fig. S19. The temperatures in both cases scale linearly with the incident solar intensity. The maximum temperatures do not change much with intensity for bare NESMD (hollow symbols in Fig. S19). The increase in ambient temperature from 20 °C (hollow upward black triangles), 25 °C (hollow green diamonds), 30 °C (hollow upward red triangles), to 35 °C (hollow blue stars) results in the increase of the maximum temperature in the system. The maximum temperatures change

significantly with ambient temperatures varying from 20 °C (upward black triangles), 25 °C (green diamonds), 30 °C (upward red triangles), to 35 °C (blue stars) with incorporation of 2" lens array with NESMD.

12. Water production rate and unit area requirements at different ambient temperatures:

Comparison of water production from NESMD with (orange) and without (dark grey) 2" lens array focusing with 4" × 16" NESMD over a period of more than 9 hours for experimental solar intensity shown in Fig. S20. The analysis gives the water production rates in $L/m^2 \cdot day$ for different ambient temperatures of 20 °C, 25 °C, 30 °C, and 35 °C. Figure S20f shows the NESMD areas needed with (orange) and without (dark grey) 2 inch multilens lens arrays at different ambient temperatures to meet the drinking water requirement for a family of 4 people(5).

To demonstrate the impact of photon redistribution on NESMD performance under different operating conditions, we theoretically model and analyze fresh water production rate from NESMD with changing lens array focal spot size, ambient temperature, and solar intensity. Purified water flux for a 4" × 8" NESMD system without a lens array (dashed black curve) and with a 2" diameter lens array with varying focal spot diameters of 15 mm (light grey triangles), 10 mm (grey triangles), and 5 mm (dark grey triangles) at varying sunlight intensities is shown in Fig. S20a. The corresponding percentage flux enhancement with the addition of a 2" lens array over the flux without a lens array for varying focal spot diameters is shown in Fig. S20b. All the curves in Fig. S20a,b are obtained for an ambient temperature of 20 °C, which is set as the feed and distillate inlet temperature. When using the lens array, lower solar intensities are needed to produce the same flux compared to the case without using a lens array, as shown in Fig. S18.

It has been previously shown that the ambient temperature affects the water production rate of NESMD(2). To further elucidate the performance of our device under the effect of varying ambient conditions, we simulated the flux produced by a 4" × 16" NESMD device with and without the addition of a lens array with increasing solar intensity as demonstrated in Fig. S20c. The flux for a 4" × 16" bare NESMD device increases with increasing ambient temperatures from 20 ºC (black hollow upward triangles), 25 ºC (green hollow diamonds), 30 ºC (red hollow downward triangles), and 35 ºC (blue hollow stars) shown with dashed lines in Fig. S20c. A similar increase in flux is observed for the device with the lens array for ambient temperatures of 20 ºC (black solid upward triangles), 25 ºC (green solid diamonds), 30 ºC (red solid downward triangles), and 35 ºC (blue solid stars) shown with solid lines in Fig. S20c. Crucially, to prevent wetting, the maximum temperatures in the system stay below 100 °C for the flux values shown (Fig. S19).

Finally, we estimate the potential flux enhancement and efficiency gained by the addition of a lens array to an NESMD device. The percentage flux enhancement at varying ambient temperatures with the addition of a lens array over the flux without a lens array, as reported in Fig. S20c, for increasing solar intensity is shown in Fig. S20d. The lens array produces a larger flux enhancement at lower ambient temperatures. This improvement points toward an important advantage of adding a lens array to NESMD systems; the photon flux redistribution ensures high performance at lower ambient temperatures. As can be seen from Fig. S20c, flux values for a system incorporating a lens array at 20 ºC can be as high as fluxes for a bare NESMD system at 35 ºC.

The purified water production rate per unit area under the naturally varying intensity of the Sun (blue dashed curve, left axis in Fig. 3c) for a 4" × 16" NESMD system without a lens array and with a 2" diameter lens array with 5 mm diameter focal spot is shown in the grey and orange areas of Fig. S20e and S20f respectively. At ambient temperature of 20 ºC, the 4" × 16" NESMD system with the 2" diameter lens array yields a water production rate of 2.79 liters/m^2·day. The rate for bare NESMD is 2.04 liters/m^2·day, indicating a ~27% reduced surface area requirement to get the same amount of water with the addition of a lens array compared to bare NESMD.

Fig. S1.

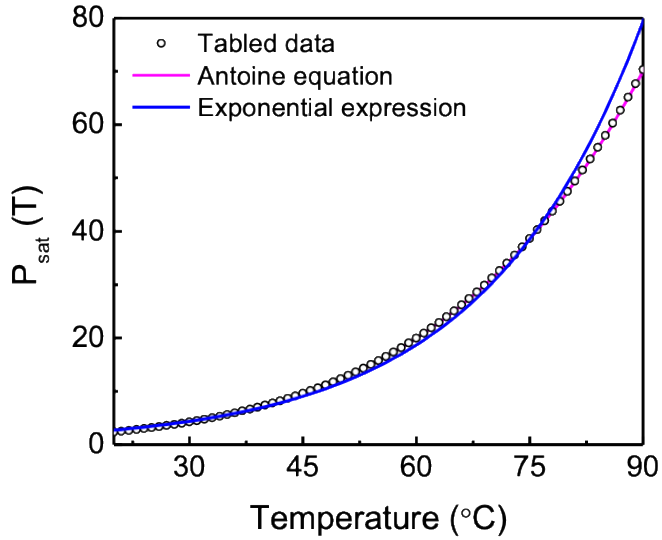

Figure S1. Water vapor saturation pressure temperature dependence. Tabled data(1) (black circles) are fitted by the Antoine Equation (solid magenta line) with parameters A=8.07131, B=1730, C=233.426 and by an exponential function (solid blue line). Inset: exponential fitting of $p_{sat}(T)$ with $\mathbf{p_0 = 1.0293\ kPa}$ and $\boldsymbol{\gamma = 0.0483\ 1}/°C$.

Fig. S2

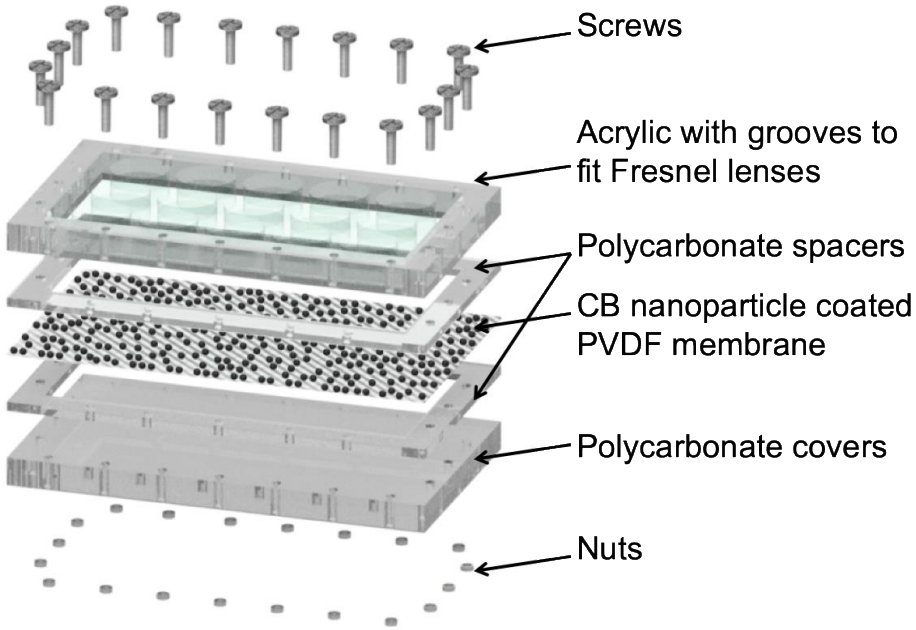

Figure S2. Fabrication of the NESMD system. Assembly of NESMD system with individual components like screws, acrylic frame with grooves to put Fresnel lenses, coated PVDF membrane and polycarbonate covers and spacers to separate feed and distillate channels.

Fig. S3

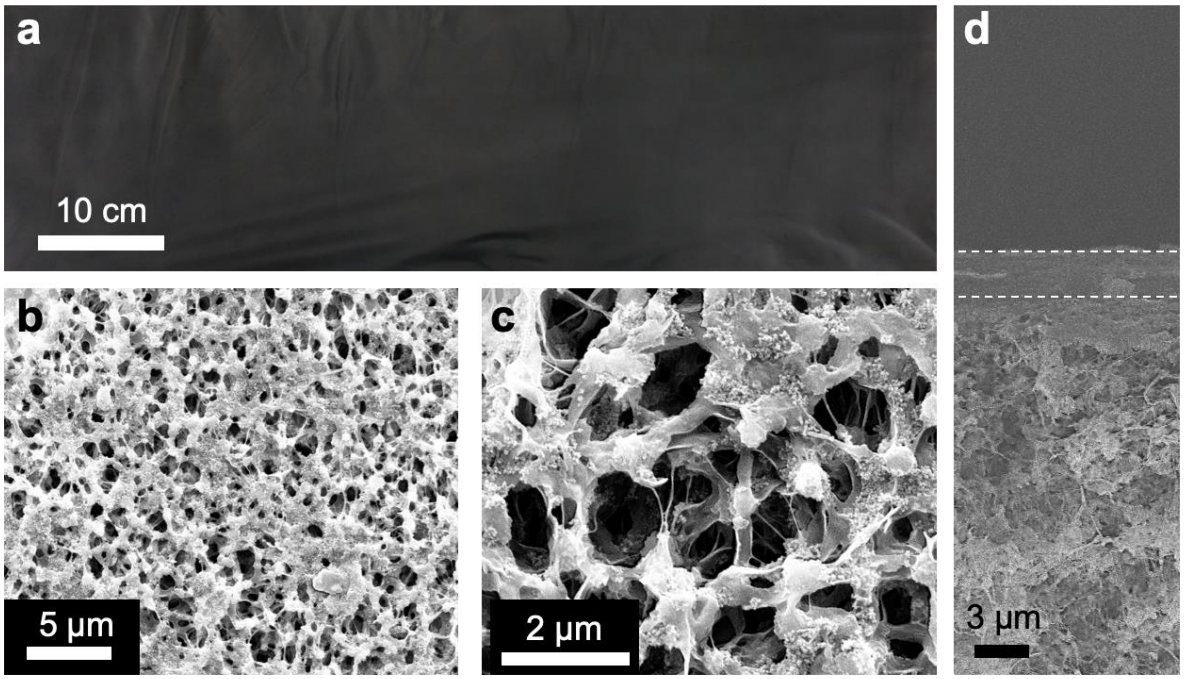

Figure S3. Scalable spray coating of PVDF membranes. (**a**) Photograph of the spray coated PVDF membrane. (**b**) and (**c**) SEM image of the surface of the spray coated PVDF membrane at different magnifications. (**d**) SEM image of the vertical cross section of the CB coated PVDF membrane shows that CB coating thickness is 3-5 microns.

Fig. S4

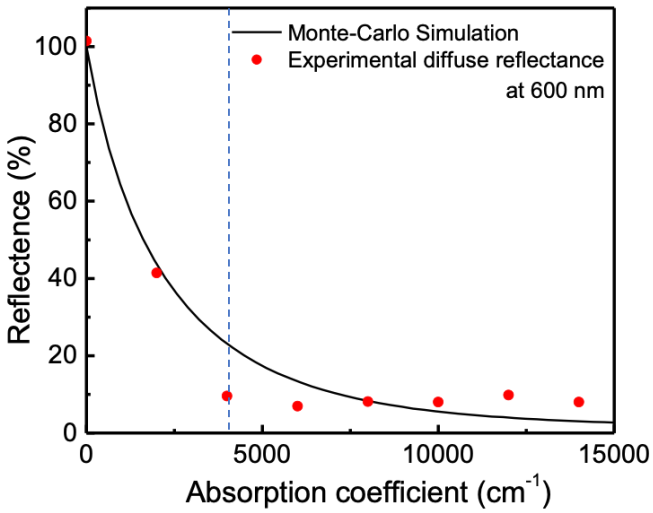

Figure S4. Optical properties of CB spray coated PVDF membranes. Comparison of experimental diffuse reflectance and Monte-Carlo simulated reflectance helps in obtaining the absorption coefficient of the CB coated membrane for varying CB loading. The dashed line corresponds to CB concentration of 0.1 mg/cm^2.

Fig. S5

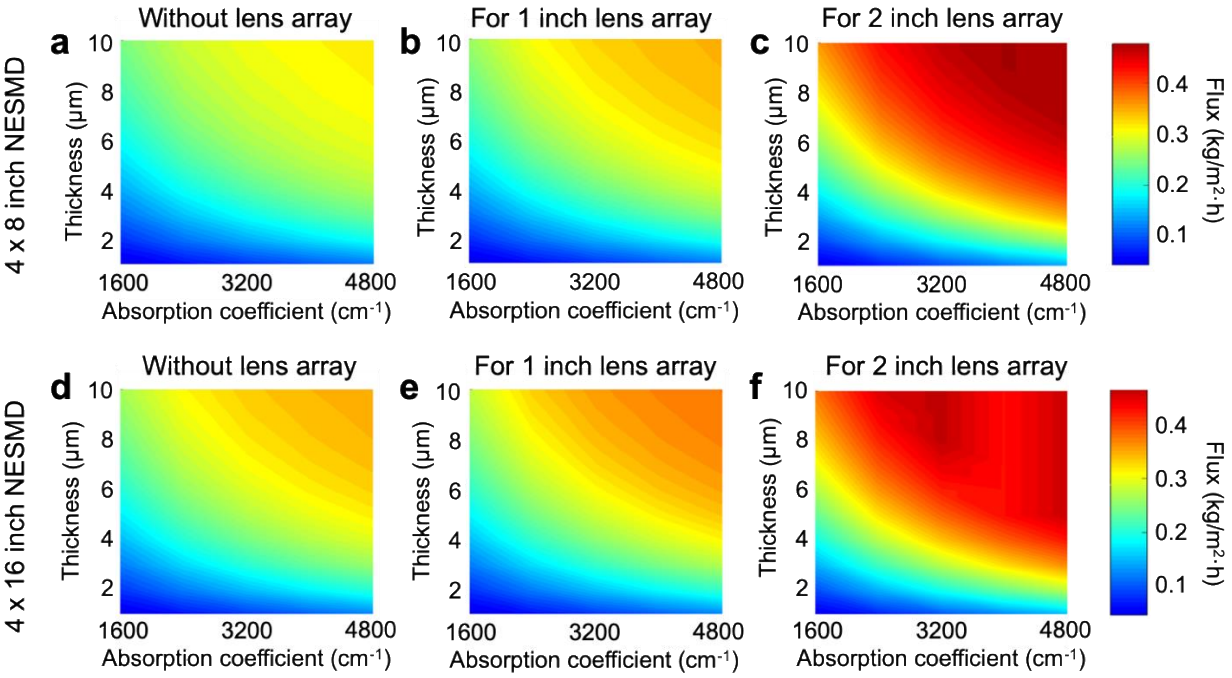

Figure S5. Effect of CB coating thickness and absorption coefficient on the membrane flux. (**a**) Calculated map of the flux with CB coating thickness and absorption coefficient without lens array, (**b**) with 1" diameter lens array, (**c**) with 2" diameter lens array for 4" × 8" NESMD system. (**d**) Calculated map of the flux with CB coating thickness and absorption coefficient without lens array, (**e**) with 1" diameter lens array, (**f**) with 2" diameter lens array for 4" × 16" NESMD system.

Fig. S6

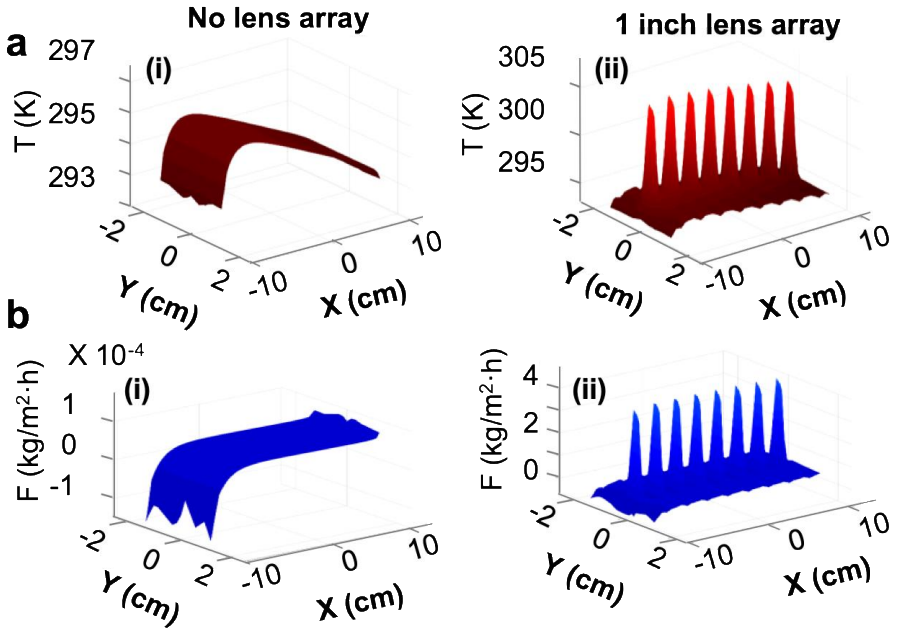

Figure S6. Temperature and flux analysis for 4" × 8" NESMD with and without lens array focusing. (**a**) Simulated temperature maps for 4" × 8" NESMD (i) without (insets show zoomed in scale) and (ii) with 1" diameter lens array focusing with 5 mm focal spots. Corresponding (**b**) flux maps for (i) bare NESMD (insets show zoomed in scale) and (ii) for NESMD with 1" diameter lens array focusing.

Fig. S7

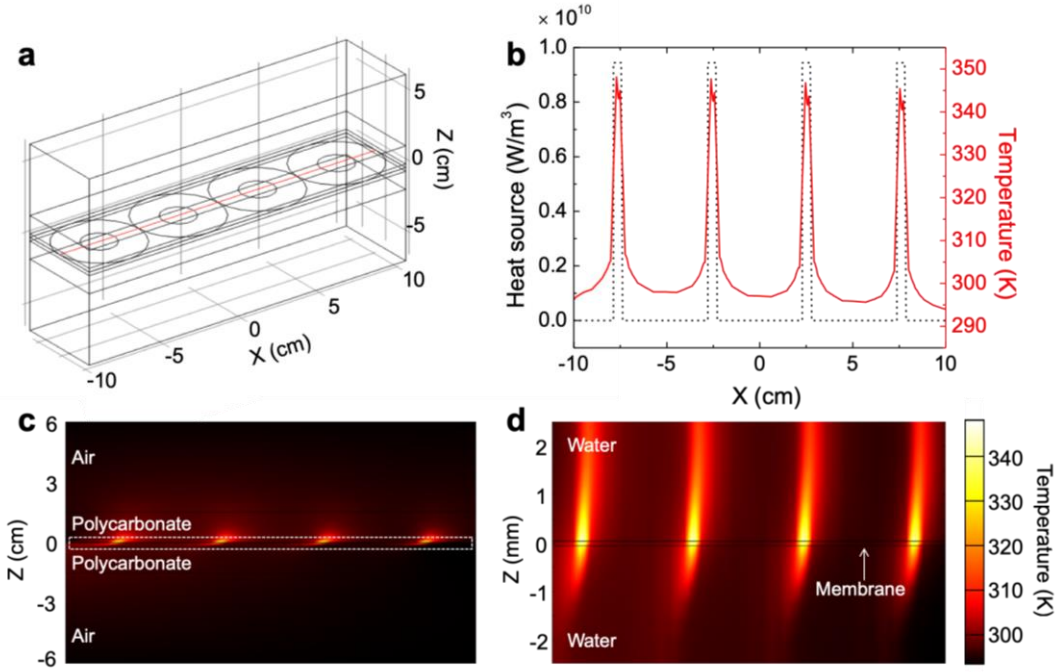

Figure S7. Temperature distribution maps along vertical Z-direction for NESMD with 2" diameter lens array. (**a**) 3 dimensional schematic showing projection of 2" diameter lenses creating 5 mm focal spots on the membrane surface. (**b**) Temperature and heat source along the line (shown in red) in (**a**) going through the centers of the focal spots along x –direction. (**c**) Cross-sectional view of the NESMD system shown in (**a**) along the centers of the focal spots in vertical z-direction shows the variation of generated temperature along in the xz plane. (**d**) Zoomed in temperature map for the inset (dashed white line) in (**c**).

Fig. S8

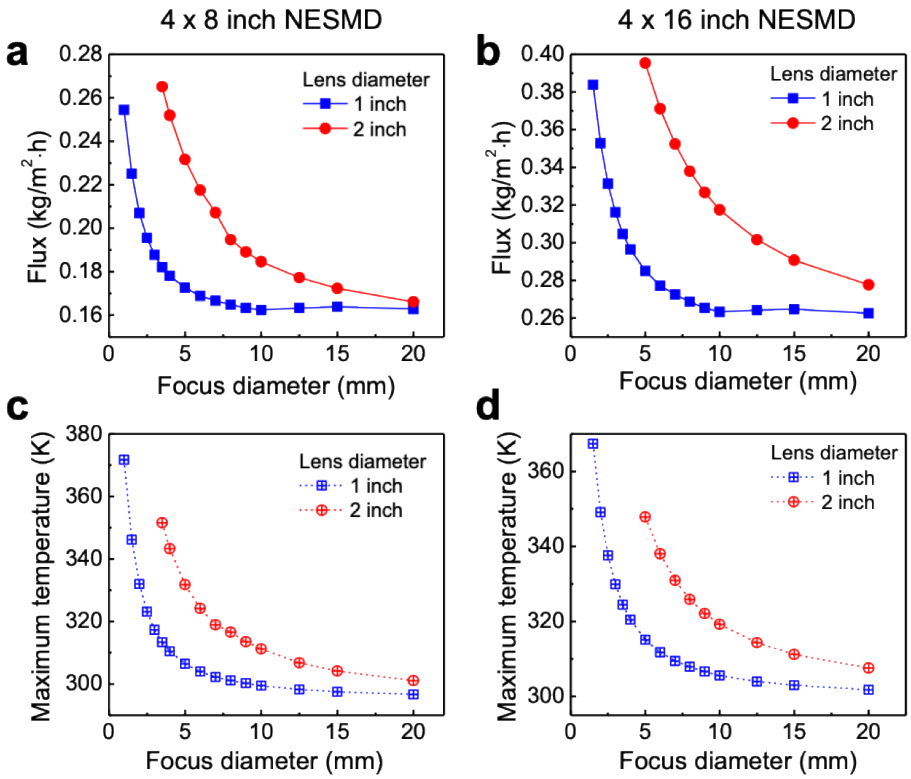

Figure S8. Effect of focal spot diameter on the average flux and maximum temperature with lens array focusing. Effect of 1" (blue) and 2" (red) diameter lens array focusing with varying focal spot diameter on the average flux from (**a**) 4" × 8" NESMD and (**b**) 4" × 16" NESMD. Effect of the same lens array focusing on the maximum temperature generated at the focal spots in the system for (**c**) 4" × 8" NESMD and (**d**) 4" × 16" NESMD.

Fig. S9

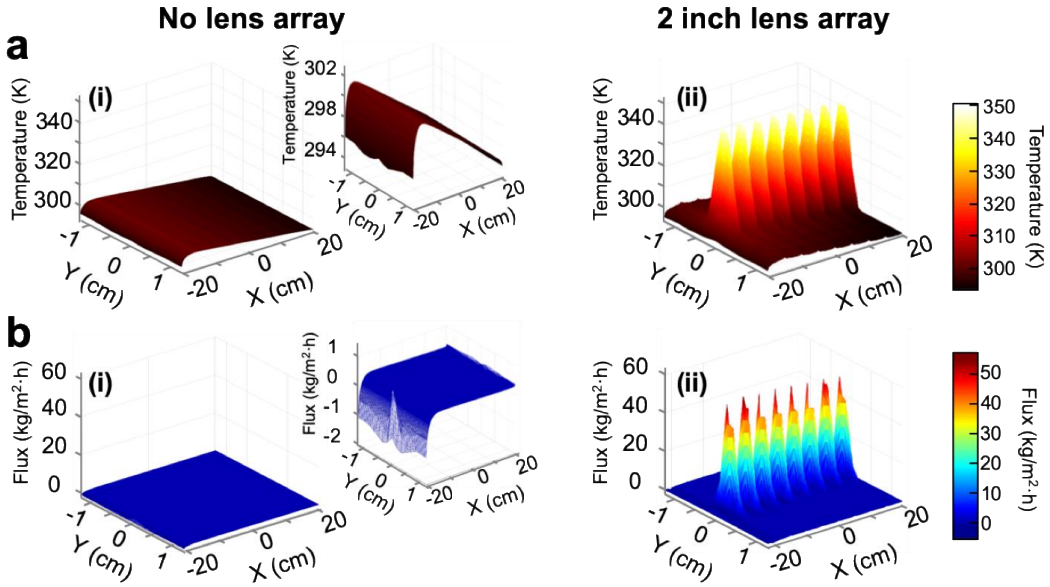

Figure S9. Temperature and flux analysis for 4” × 16” **NESMD with and without lens array focusing.** (**a**) Simulated temperature maps for 4” × 16” NESMD (i) without (insets show zoomed in scale) and (ii) with 2” diameter lens array focusing with 5 mm focal spots. Corresponding (**b**) flux maps for (i) bare NESMD (insets show zoomed in scale) and (ii) for NESMD with 2” diameter lens array focusing.

Fig. S10

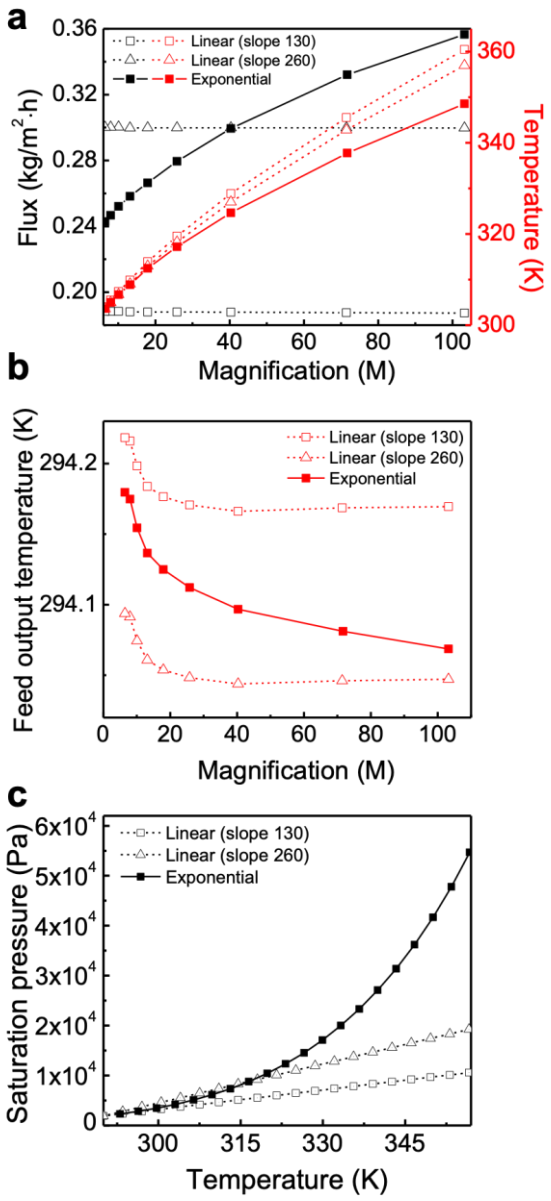

Figure S10. Effect of magnification (M) on flux and temperatures with linear and exponential temperature dependence of saturation pressure. (**a**) Effect of M on flux through the system for linear dependence of saturation pressure of water vapor on temperature for different slopes of 130 (Black dashed line with hollow squares) and 260 (Black dashed line with hollow triangles) and exponential dependence (Solid black line with solid squares). The corresponding temperatures (right axis) for the linear case with different slopes of 130 (dashed red line with hollow squares) and 260 (dashed red line with hollow triangles) and exponential case (solid red line with solid squares). (**b**) Feed output temperature dependence on M and (**c**) saturation pressure dependence on temperature for linear dependence case with different slopes of 130 (dashed red line with hollow squares) and 260 (dashed red line with hollow triangles) and exponential case (solid red line with solid squares). The system considered here has dimensions of 4”× 8”.

Fig. S11

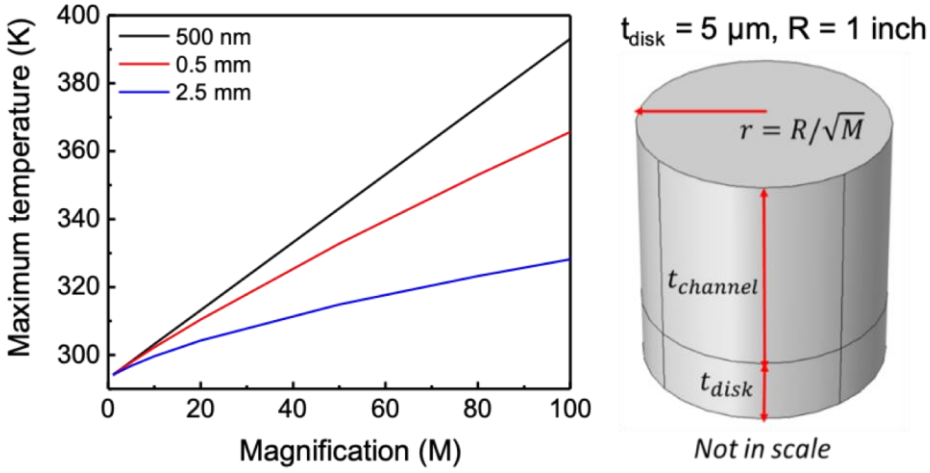

Figure S11. Maximum temperature vs. magnification (M) for thin water disk (t_{disk}=5µm) and radius $r = R/\sqrt{M}$ in contact with a second cylinder of varying height $t_{channel}$ equal to 500nm (blue), 0.5mm (green) and 2.5mm (red) respectively. The thin disk is heated through a homogeneous heat source $Q_{abs} = Q_0 M$ with $Q_0 = 1 MW/m^3$.

Fig. S12

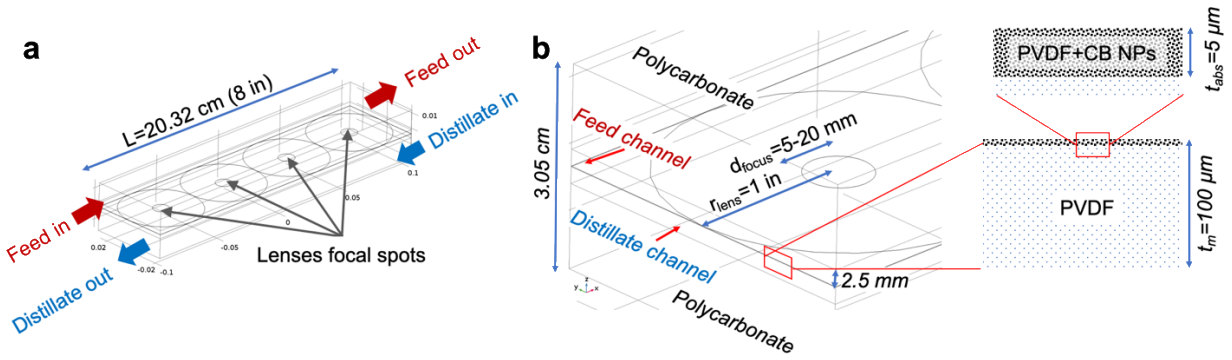

Figure S12. Scheme of the modeled device. (**a**) Device domains with highlighted feed and distillate fluxes (blue and light blue arrows respectively). An example of 8 in NESMD+lenses module is presented. Lenses effect is accounted for by means of a redistribution of heat dissipation. (**b**) Zoomed view of the module feed inlet and distillate outlet section. The considered materials are polycarbonate, water and PVDF. Typical lenses and channels dimensions are reported. Inset shows scheme of the cross section of the PVDF with embedded Carbon Black (CB) Nanoparticles (NPs).

Fig. S13

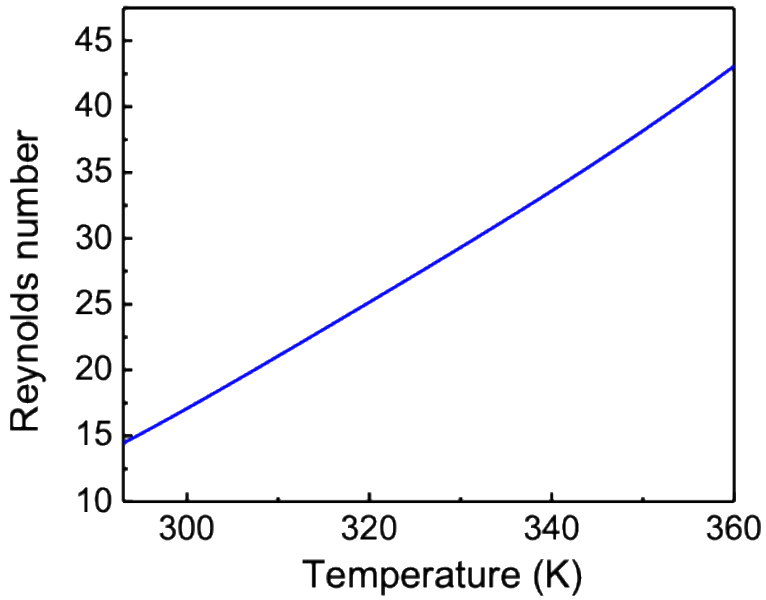

Figure S13. Calculated Reynolds number for the distillate flow (the fastest) in our system.

Fig. S14

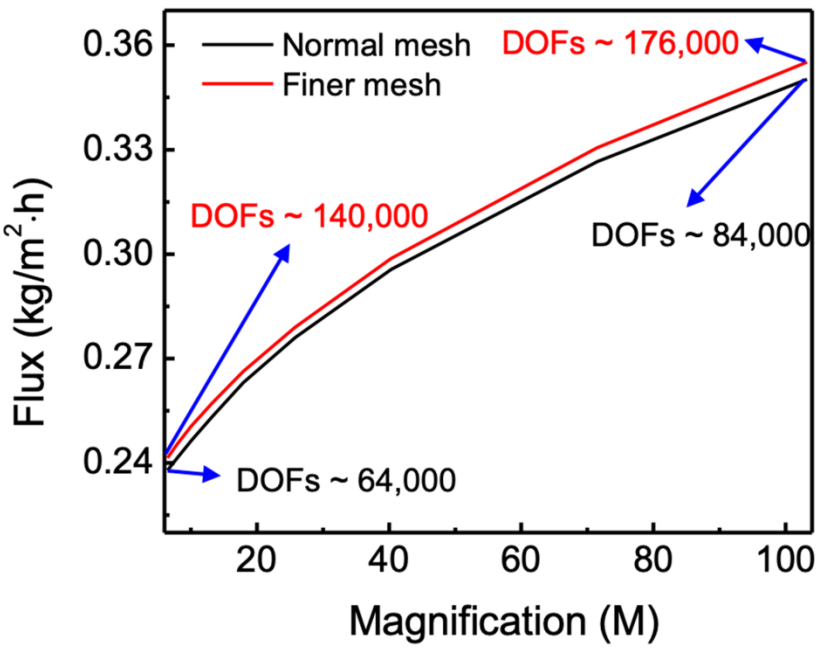

Figure S14. Model convergence for the 4x8in module with 2 in lenses and varying focusing size. An increase of the mesh elements leading to more than doubling the degrees of freedom (DOFs) induces an error on the final flux rate of less than 2% in the worst case (largest M). Computational time is 4 times longer for the case of finer mesh.

Fig. S15

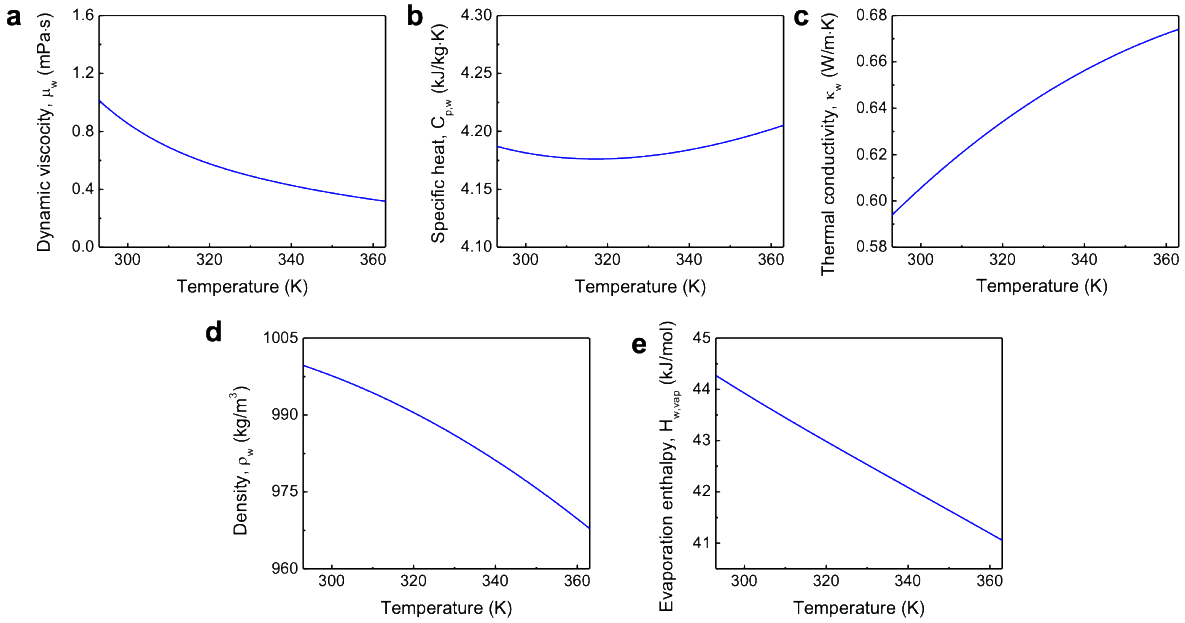

Figure S15. Temperature dependence between 293 K and 363 K (20 °C and 90 ºC) of water parameters utilized in the model. a – Dynamic viscosity, **b** – Specific heat at constant pressure(1), **c** – Thermal conductivity(6), **d** - Density(1), **e** – Enthalpy of vaporization(7).

Fig. S16

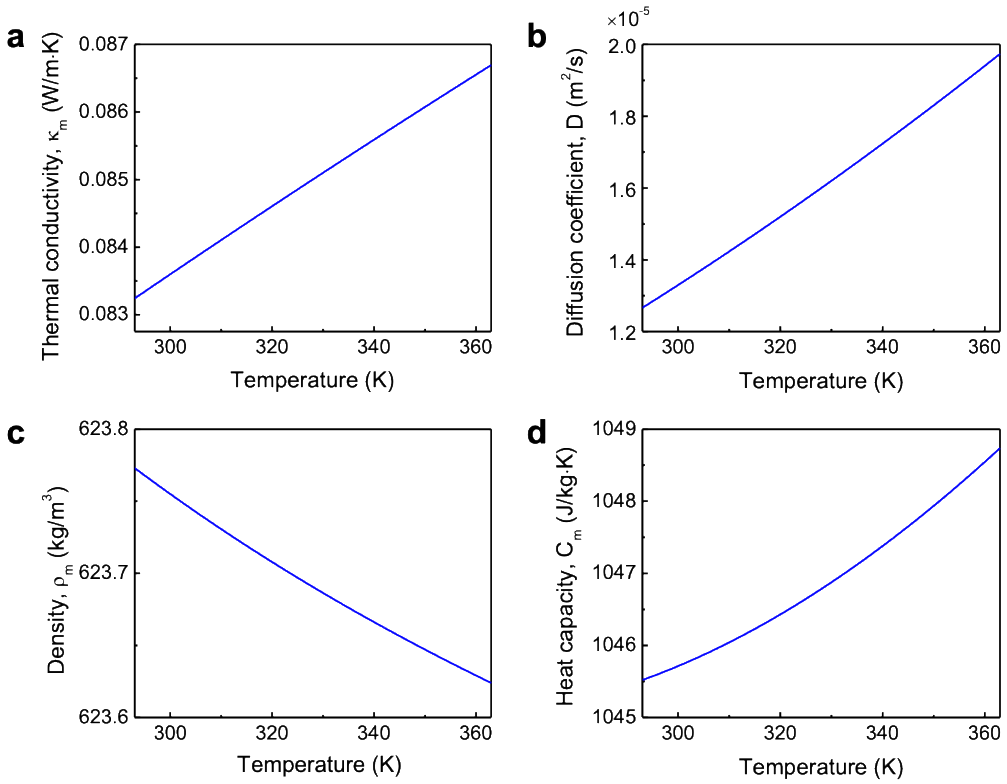

Figure S16. Temperature dependence between 293 K and 363 K (20 °C and 90 ºC) of the PVDF membrane utilized in the model. a – Thermal conductivity, **b** – Vapor diffusion coefficient, **c** – Density, **d** – Heat Capacity. Additional details on these parameters can be found in our previous work where NESMD is introduced(2).

Fig. S17

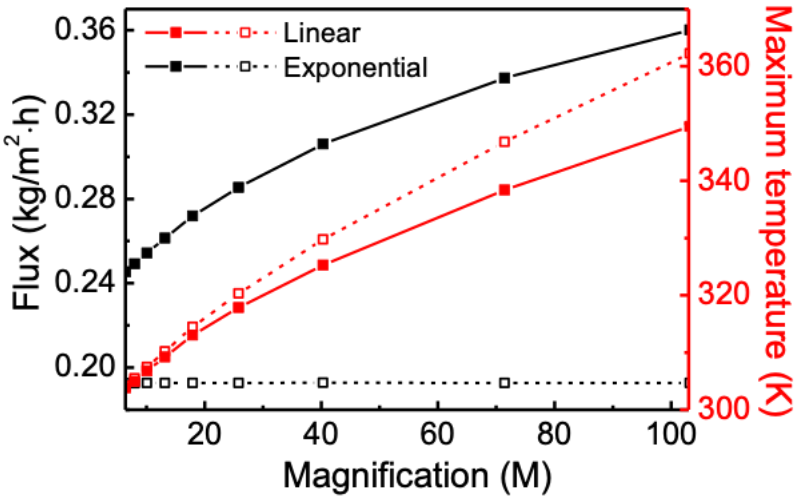

Figure S17. Flux rate (blue) and maximum temperature reached by the device (red) vs. magnification (M) for the conventional (nearly exponential, EXP) (solid) and for the artificial (linearized, LIN) water vapor pressure temperature dependence (dashed) respectively. The curves have been obtained in the case where all the temperature dependent parameters are set to room temperature of 20 ºC. The trend matches very well to what reported in the main text where all parameters are temperature dependent.

Fig. S18

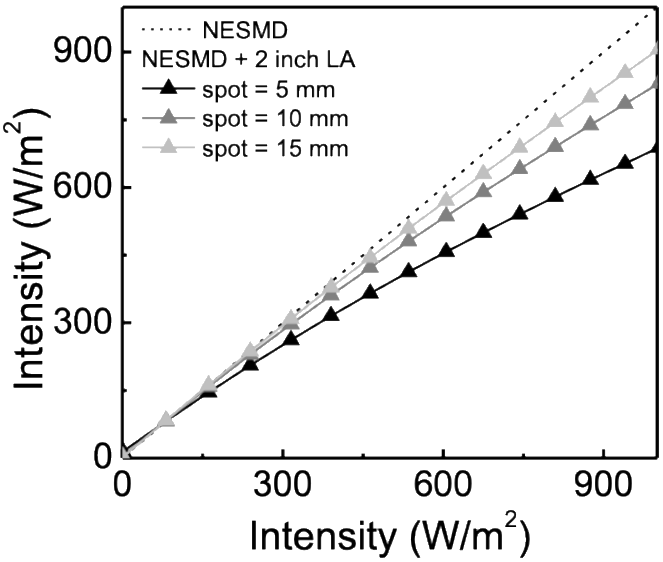

Figure S18. Intensity comparison for the same flux with and without multilens array focusing. The intensity needed for 4" × 8" NESMD to obtain the same flux with (left axis) vs without (bottom) lens array focusing with 2" diameter lens array. The curves for different focal spot diameters of 15 mm (light grey triangles), 10 mm (grey triangles), and 5 mm (dark grey triangles) show reduction in the intensity needed with lens array incorporation and increasing magnification.

Fig. S19

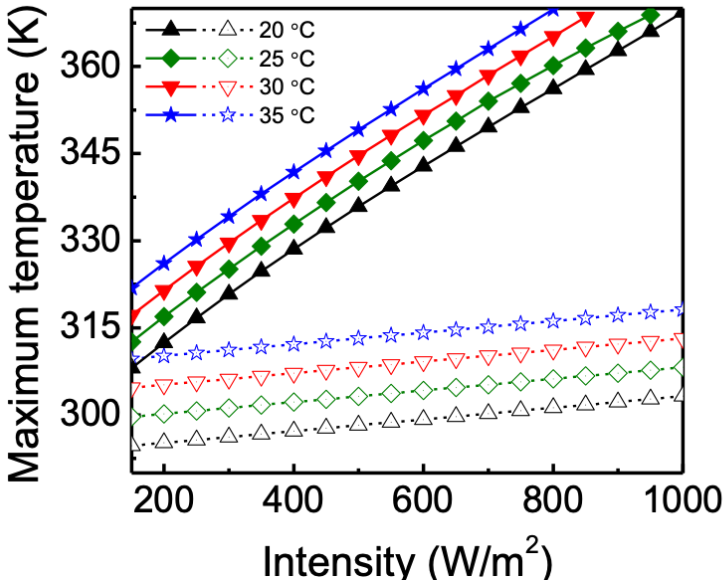

Figure S19. Effect of incident intensity on maximum temperature with and without multilens focusing. The maximum temperature in the system increases almost linearly with increasing intensity with (solid) and without (hollow) incorporation of 2" lens array with 5 mm diameter focal spots with 4" × 16" NESMD different ambient temperatures of 20 °C (upward black triangles), 25 °C (green diamonds), 30 °C (upward red triangles), and 35 °C (blue stars).

Fig. S20

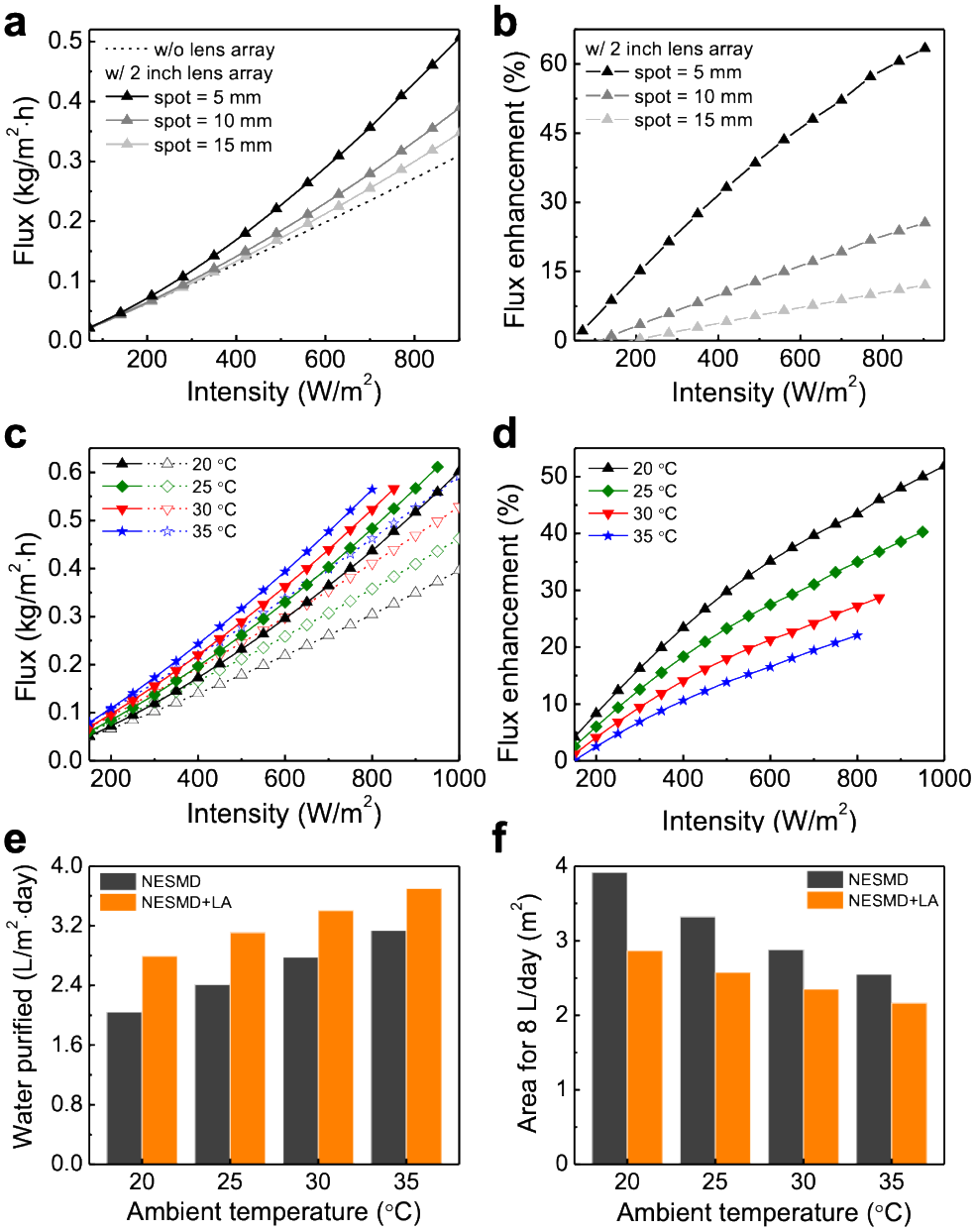

Figure S20. Water production over a day with and without multilens array focusing with different ambient temperatures. (**a**) Comparison of simulated performance of 4" × 8" NESMD system at varying solar intensities without lens array (black dashed line) and with 2" diameter lens array with varying focal spot diameters of 15 mm (light grey triangles), 10 mm (grey triangles) and 5 mm (dark grey triangles). (**b**) The corresponding flux enhancement with addition of a lens array over the flux without the lens array for increasing solar intensities. (**c**) Simulated purified water flux for a 4" × 16" bare NESMD at different ambient temperatures of 20 ˚C (hollow black upward triangles), 25 ˚C (hollow green diamonds), 30 ˚C (hollow red downward triangles) and 35 ˚C (hollow blue stars). The corresponding flux for the 4" × 16" NESMD with 2" diameter lens array with 5 mm focal spots at different ambient temperatures of 20 ˚C (black upward triangles), 25 ˚C (green diamonds), 30 ˚C (red downward triangles) and 35 ˚C (blue

stars). (**d**) The corresponding enhancement to the NESMD flux with the addition of a lens array at varying ambient temperatures of 20 ˚C (black upward triangles), 25 ˚C (green diamonds), 30 ˚C (red downward triangles) and 35 ˚C (blue stars). (**e**) Water production in $L/m^2 \cdot day$ from bare NESMD (dark grey) and NESMD with 2 inch multilens array with 5 mm focal spots (orange) at different ambient temperatures. (**f**) The areas of bare NESMD (dark grey) and NESMD with 2 inch multilens array focusing with 5 mm focal spots (orange) needed to meet drinking water requirements of a family of 4 people per day at different ambient temperatures.

References

1. Lide DR (2003) CRC Handbook of Chemistry and Physics, 84th Edition, 2003-2004. *Handb Chem Phys*. doi:10.1136/oem.53.7.504.
2. Dongare PD, et al. (2017) Nanophotonics-enabled solar membrane distillation for off-grid water purification. *Proc Natl Acad Sci*. doi:10.1073/pnas.1701835114.
3. Hanks RW, Ruo HC (1966) Laminar-turbulent transition in ducts of rectangular cross section. *Ind Eng Chem Fundam*. doi:10.1021/i160020a022.
4. R. Byron Bird Warren E. Stewart Edwin N. Lightfoo, Bird RB, Stewart WE, Lightfoot EN (2006) *Transport Phenomena, Revised 2nd Edition* doi:10.1002/aic.690070245.
5. Gleick P (1996) Basic Water Requirements for Human Activities: Meeting Basic Needs. *Water Int* 21(2):83–92.
6. Ramires MLV, et al. (1995) Standard Reference Data for the Thermal Conductivity of Water. *J Phys Chem Ref Data*. doi:10.1063/1.555963.
7. Somayajulu GR (1988) New equations for enthalpy of vaporization from the triple point to the critical point. *Int J Thermophys*. doi:10.1007/BF00503155.